

Chapter 2

Theoretical Background

2.1 The Schrödinger Equation

Any computational approach to study the properties of molecular systems needs to deal with the Schrödinger equation [1], which describes the dynamics in non-relativistic quantum mechanics. A brief summary of the approximations necessary to run molecular simulations within reasonable periods of time is given in the following sections. It follows several standard textbooks [2–5], so the educated reader might directly continue with Chap. 3.

The general time-dependent form of the Schrödinger equation in Dirac notation reads as

$$\mathcal{H} |\Phi(t)\rangle = i\hbar \frac{\partial}{\partial t} |\Phi(t)\rangle, \quad (2.1)$$

where \mathcal{H} is the Hamiltonian and $|\Phi(t)\rangle$ is a state vector in the Hilbert space of all possible quantum states of the particular system. If the Hamiltonian does not explicitly depend on the time t and $|\Phi(t)\rangle$ is a stationary state, the time dependence can be separated by the ansatz

$$|\Phi(t)\rangle = \exp\left(-\frac{i}{\hbar}Et\right) |\Psi\rangle, \quad (2.2)$$

where $|\Psi\rangle$ is an eigenstate of \mathcal{H} , so it fulfills the time-independent Schrödinger equation

$$\mathcal{H} |\Psi\rangle = E |\Psi\rangle \quad (2.3)$$

with the energy eigenvalue E .

In a molecular system that consists of N electrons and M nuclei, the Hamiltonian is commonly chosen to include the kinetic energy of the electrons \mathcal{T}_e , the kinetic energy of the nuclei \mathcal{T}_n , the Coulomb repulsion between the electrons \mathcal{V}_{ee} , the Coulomb attraction of the nuclei and the electrons \mathcal{V}_{ne} , and the Coulomb repulsion between the nuclei \mathcal{V}_{nn} :

$$\begin{aligned}
\mathcal{H} &= \mathcal{T}_e + \mathcal{T}_n + \mathcal{V}_{ee} + \mathcal{V}_{ne} + \mathcal{V}_{nn} \\
&= - \sum_{i=1}^N \frac{\hbar^2}{2m_e} \nabla_i^2 - \sum_{A=1}^M \frac{\hbar^2}{2M_A} \nabla_A^2 + \frac{e^2}{4\pi\epsilon_0} \left(\sum_{i=1}^N \sum_{j=i+1}^N \frac{1}{r_{ij}} - \sum_{i=1}^N \sum_{A=1}^M \frac{Z_A}{r_{iA}} + \sum_{A=1}^M \sum_{B=A+1}^M \frac{Z_A Z_B}{r_{AB}} \right).
\end{aligned} \tag{2.4}$$

In this equation, M_A and Z_A denote the mass and the atomic number of nucleus A , respectively, as well as $r_{ij} = |\mathbf{r}_i - \mathbf{r}_j|$, $r_{iA} = |\mathbf{r}_i - \mathbf{R}_A|$, and $r_{AB} = |\mathbf{R}_A - \mathbf{R}_B|$ represent the respective distances between electrons and nuclei. The coordinates of electron i and nucleus A are given by \mathbf{r}_i and \mathbf{R}_A , respectively.

The electronic and the nuclear motion can be separated within the Born–Oppenheimer approximation [6]. The total molecular wave function $\Psi(\mathbf{r}, \mathbf{R})$, which depends on the sets of all electronic coordinates $\mathbf{r} = \{\mathbf{r}_i\}$ and nuclear coordinates $\mathbf{R} = \{\mathbf{R}_i\}$, is expanded by

$$\Psi(\mathbf{r}, \mathbf{R}) = \sum_{k=0}^{\infty} \psi_k(\mathbf{r}; \mathbf{R}) \chi_k(\mathbf{R}), \tag{2.5}$$

where the electronic wave functions $\psi_k(\mathbf{r}; \mathbf{R})$ are assumed to form a complete set of eigenfunctions of the electronic Hamiltonian $\mathcal{H}_e = \mathcal{T}_e + \mathcal{V}_{ee} + \mathcal{V}_{ne} + \mathcal{V}_{nn}$ and fulfill—for fixed nuclear positions \mathbf{R} —the electronic Schrödinger equation

$$\mathcal{H}_e \psi_k(\mathbf{r}; \mathbf{R}) = E_k(\mathbf{R}) \psi_k(\mathbf{r}; \mathbf{R}) \tag{2.6}$$

with the electronic energy $E_k(\mathbf{R})$. The nuclear wave functions $\chi_k(\mathbf{R})$ can be seen as expansion coefficients that depend on the nuclear positions. Using this ansatz for the time-independent Schrödinger equation (2.3) with the molecular Hamiltonian (2.4) and integrating out the electronic coordinates, leads to the set of coupled equations

$$\left(- \sum_{A=1}^M \frac{\hbar^2}{2M_A} \nabla_A^2 + E_k(\mathbf{R}) \right) \chi_k(\mathbf{R}) + \sum_{l=0}^{\infty} C_{kl} \chi_l(\mathbf{R}) = \varepsilon_k \chi_k(\mathbf{R}) \tag{2.7}$$

with the energy ε_k and the coupling operator

$$C_{kl} = - \sum_{A=1}^M \frac{\hbar^2}{2M_A} \langle \psi_k(\mathbf{r}; \mathbf{R}) | \nabla_A^2 | \psi_l(\mathbf{r}; \mathbf{R}) \rangle_{\mathbf{r}} - \sum_{A=1}^M \frac{\hbar^2}{M_A} \langle \psi_k(\mathbf{r}; \mathbf{R}) | \nabla_A | \psi_l(\mathbf{r}; \mathbf{R}) \rangle_{\mathbf{r}} \nabla_A. \tag{2.8}$$

Within the Born–Oppenheimer approximation, all coupling terms are neglected, resulting in the nuclear Schrödinger equation

$$\left(- \sum_{A=1}^M \frac{\hbar^2}{2M_A} \nabla_A^2 + E_k(\mathbf{R}) \right) \chi_k(\mathbf{R}) = \varepsilon_k \chi_k(\mathbf{R}). \tag{2.9}$$

This effectively means to assume that the gradients of the electronic wave function along the nuclear coordinates in Eq. (2.8) vanish, so the electronic wave function is influenced only by the positions of the nuclei but not by their momenta, and the nuclei move without changing the quantum state of the electrons. This is usually justifiable if the electronic states are separated well in energy. However, the approximation breaks down if two potential energy surfaces get close. This is often important, e.g., for photochemical processes, but such phenomena are not investigated in this thesis.

By the separation of electronic and nuclear motion, the Schrödinger equation is divided into two individual problems. For each nuclear configuration \mathbf{R} , the electronic energy $E_k(\mathbf{R})$ can be calculated by solving the electronic Schrödinger equation (2.6). This defines a potential energy surface, on which the nuclei behave according to the nuclear Schrödinger equation (2.9). A common method to solve the electronic Schrödinger equation is density functional theory (DFT), which is discussed in Sect. 2.2. Afterwards, the obtained electronic energy is used to treat the nuclear Schrödinger equation with further approximations that are described in Sect. 2.3.

2.2 Density Functional Theory

2.2.1 Hohenberg–Kohn Theorems and Kohn–Sham Method

Density functional theory (DFT) is a widely used method to solve the electronic Schrödinger equation, and it is founded on the Hohenberg–Kohn theorems [7]. The first Hohenberg–Kohn theorem states that the electronic ground-state wave function is uniquely determined by the ground-state electron density. The unique determination of the wave function also defines any further molecular property such as, e.g., the electronic ground-state energy. Thus, it is sufficient to calculate the electron density instead of the wave function. The advantage of the electron density is that it only depends on three spatial coordinates, whereas the wave function depends on the spatial and the spin coordinates of all N electrons.

In analogy to the electronic Hamiltonian \mathcal{H}_e defined for Eq. (2.6), the electronic energy is written as a functional of the electron density:

$$E[\rho(\mathbf{r})] = T[\rho(\mathbf{r})] + V_{ee}[\rho(\mathbf{r})] + V_n[\rho(\mathbf{r})]. \quad (2.10)$$

The last term in this sum,

$$V_n[\rho(\mathbf{r})] = \int \rho(\mathbf{r}) v_{\text{ext}}(\mathbf{r}) \, \mathrm{d}\mathbf{r}, \quad (2.11)$$

is the only one that depends on the nuclear coordinates, as it contains the Coulomb attraction of the nuclei and the electrons as well as the nuclear Coulomb repulsion in the external potential

$$v_{\text{ext}}(\mathbf{r}) = \frac{e^2}{4\pi\epsilon_0} \left(- \sum_{A=1}^M \frac{Z_A}{|\mathbf{r} - \mathbf{R}_A|} + \sum_{A=1}^M \sum_{B=A+1}^M \frac{Z_A Z_B}{|\mathbf{R}_A - \mathbf{R}_B|} \right). \quad (2.12)$$

The other two functionals, the kinetic energy $T[\rho(\mathbf{r})]$ and the electron–electron interaction $V_{\text{ee}}[\rho(\mathbf{r})]$, are universal expressions that are valid for any system. Unfortunately, their general form is hitherto unknown.

The second Hohenberg–Kohn theorem introduces the variational principle to DFT. According to that, the energy of any trial electron density is never lower than the exact ground-state energy. It is therefore possible to find the exact ground-state electron density by varying a trial electron density until the energy reaches the global minimum.

A widely used approach to actually calculate the electron density in DFT is the Kohn–Sham method [8]. Within this technique, a fictitious system of noninteracting electrons is considered, the electron density $\rho_s(\mathbf{r})$ of which is equal to the one of the real system $\rho(\mathbf{r})$. The noninteracting electrons occupy the auxiliary Kohn–Sham orbitals $\theta_i(\mathbf{r})$, and the electron density is formed according to

$$\rho_s(\mathbf{r}) = \rho(\mathbf{r}) = e \sum_{i=1}^N |\theta_i(\mathbf{r})|^2. \quad (2.13)$$

Since the overall wave function of this system is exactly given by a single Slater determinant of Kohn–Sham orbitals, the kinetic energy is equal to

$$T_s[\{\theta_i(\mathbf{r})\}] = -\frac{\hbar^2}{2m_e} \sum_{i=1}^N \langle \theta_i(\mathbf{r}) | \nabla^2 | \theta_i(\mathbf{r}) \rangle. \quad (2.14)$$

If also the classical Coulomb repulsion

$$J[\rho(\mathbf{r})] = \frac{1}{4\pi\epsilon_0} \frac{1}{2} \iint \frac{\rho(\mathbf{r}_1)\rho(\mathbf{r}_2)}{|\mathbf{r}_1 - \mathbf{r}_2|} d\mathbf{r}_1 d\mathbf{r}_2 \quad (2.15)$$

is separated from the total electron–electron interaction $V_{\text{ee}}[\rho(\mathbf{r})]$, the electronic energy (2.10) can be rewritten as

$$E[\{\theta_i(\mathbf{r})\}] = T_s[\{\theta_i(\mathbf{r})\}] + J[\rho(\mathbf{r})] + E_{\text{xc}}[\rho(\mathbf{r})] + V_{\text{n}}[\rho(\mathbf{r})]. \quad (2.16)$$

The exchange–correlation energy functional $E_{\text{xc}}[\rho(\mathbf{r})]$ collects all unknown contributions to the energy, in particular the kinetic correlation energy, the exchange energy, the Coulombic correlation energy and the self-interaction correction.

Based on the second Hohenberg–Kohn theorem, the Kohn–Sham orbitals are found by minimizing the electronic energy with respect to the orbitals. As a constraint to this minimization, the orbitals are required to be orthonormal. Applying the method of Lagrange multipliers, this leads to the Kohn–Sham equations

$$\left(-\frac{\hbar^2}{2m_e} \nabla^2 + v_{\text{ext}}(\mathbf{r}) + \frac{1}{4\pi\epsilon_0} \int \frac{\rho(\mathbf{r}_1)}{|\mathbf{r} - \mathbf{r}_1|} d\mathbf{r}_1 + \frac{\delta E_{\text{xc}}[\rho(\mathbf{r})]}{\delta \rho(\mathbf{r})} \right) \theta_i(\mathbf{r}) = \epsilon_i \theta_i(\mathbf{r}) \quad (2.17)$$

with the orbital energies ϵ_i . Because the Coulomb potential and the exchange-correlation energy depend through the electron density on the orbitals, the Kohn–Sham equations are nonlinear and are, therefore, commonly solved iteratively. The traditional diagonalization approach to this problem is discussed in Sect. 2.2.3. Another method that relies on a direct minimization of the electronic energy is mentioned in Sect. 2.2.4.

2.2.2 Approximate Exchange-Correlation Functionals

Up to this point, DFT would provide an exact solution of the electronic Schrödinger equation. However, the correct exchange-correlation functional $E_{\text{xc}}[\rho(\mathbf{r})]$ is hitherto unknown, so approximations have to be made. For this purpose, the functional is usually divided into an exchange part and a correlation part:

$$E_{\text{xc}}[\rho(\mathbf{r})] = E_{\text{x}}[\rho(\mathbf{r})] + E_{\text{c}}[\rho(\mathbf{r})]. \quad (2.18)$$

In principle, it would be possible to evaluate the exchange part in the same way as in the Hartree–Fock method using the Kohn–Sham orbitals, but in connection with approximations to the correlation part, this exact exchange often yields poor results for the molecular properties. Other approaches that benefit from a successful cancellation of errors and, furthermore, avoid the evaluation of costly exchange integrals are therefore very popular.

A simple model for the exchange-correlation energy is the local density approximation (LDA), which assumes that the electron density is a slowly varying function, so it can locally be treated as a uniform electron gas. In this case, an exact expression for the exchange energy can be derived [9, 10]:

$$E_{\text{x}}^{\text{LDA}}[\rho(\mathbf{r})] = -\frac{9\alpha}{8} \left(\frac{3}{\pi} \right)^{\frac{1}{3}} \int \rho^{\frac{4}{3}}(\mathbf{r}) d\mathbf{r}, \quad \text{where} \quad \alpha = \frac{2}{3}. \quad (2.19)$$

Even for this simple system, it is impossible to give an analytic expression for the correlation energy, but it can accurately be determined by quantum Monte Carlo simulations. An analytic fitting formula to the results of these simulations has been developed by Vosko, Wilk, and Nusair (VWN) [11]. Neglecting the correlation part and taking only the exchange part (2.19) results in the X_{α} method proposed by Slater [12], where differing prefactors of $\alpha = 1$ and $\alpha = 3/4$ are used for better agreement with experimental results. The LDA is easily extended to open shell systems in terms of the local spin density approximation (LSDA) [11, 12].

Because the assumption of a uniform electron gas does not provide a good description of typical molecular systems, more advanced exchange-correlation functionals depend on the gradient of the electron density. This is called generalized gradient approximation (GGA). Common examples of GGA functionals are Becke's exchange functional (B) [13] and the correlation functional of Lee, Yang, and Parr (LYP) [14], which can be combined to form the exchange-correlation functional BLYP. Both parts of this functional contain empirical parameters fitted to Hartree–Fock data of noble gases. In the exchange-correlation functional of Perdew and Wang (PW91) [15] and its successor functional of Perdew, Burke, and Ernzerhof (PBE) [16], no fitting to existing data is performed and the parameters are chosen to fulfill some general theoretical requirements instead. The basic idea of GGA functionals is extended in meta-GGA functionals, which depend on higher derivatives of the electron density, such as, e.g., the exchange-correlation functional of Tao, Perdew, Staroverov, and Scuseria (TPSS) [17].

As mentioned before, it is in principle possible to use the Kohn–Sham orbitals for calculating the exchange part as in Hartree–Fock theory. In a system of noninteracting electrons, this would provide the exact exchange-correlation energy as there is no correlation energy. Based on the adiabatic connection method, hybrid functionals take the exact exchange for a part of the exchange-correlation energy while the remainder is calculated using the pure functionals from above. The amount of exact exchange constitutes another empirical parameter that has to be chosen. Very common are Becke's three-parameter functionals (B3). The originally proposed one utilized the B exchange and the correlation part of PW91. Its general form reads as

$$E_{xc}^{B3PW91} = (1 - a - b)E_x^{LSDA} + aE_x^{exact} + bE_x^B + (1 - c)E_c^{LSDA} + cE_c^{PW91}. \quad (2.20)$$

The parameters were optimized to $a = 0.20$, $b = 0.72$ and $c = 0.81$ by fitting to experimental data [18]. Later on, PW91 was replaced by LYP in the correlation part to create the B3LYP functional, but the parameters a , b , and c were kept at the same values [19]. In the same way as B3LYP is connected to the BLYP functional, the PBE0 functional has been developed as a hybrid version of PBE [20]. However, in PBE0 the amount of exact exchange is fixed at 25 % according to arguments from perturbation theory. Therefore, it does not contain any parameters fitted to experimental data and is given by

$$E_{xc}^{PBE0} = \frac{1}{4}E_x^{exact} + \frac{3}{4}E_x^{PBE} + E_c^{PBE}. \quad (2.21)$$

Also hybrid versions of meta-GGA functionals have been developed, such as, e.g., TPSSH that combines TPSS with 10% of exact exchange [21].

A common deficiency of the above mentioned exchange-correlation functionals is the lack of a proper description of dispersion interactions. Several approaches to include also these effects have been proposed. Beside, e.g., nonlocal van der Waals functionals [22, 23] and dispersion-corrected atom-centered potentials [24, 25], the DFT-D technique [26–28] is widely applied. In this method, an empirical correction term is added to the final energy of the system, which has the general form

$$E_{\text{disp}} = - \sum_{A=1}^M \sum_{B=A+1}^M \sum_{n=6,8,10,\dots} C_n^{AB} s_n \frac{1}{r_{AB}^n} f_{\text{damp}}(r_{AB}), \quad (2.22)$$

where the sum over all atom pairs (A, B) is taken, C_n^{AB} denotes the averaged n th-order dispersion coefficient of atom pair (A, B) , $r_{AB} = |\mathbf{R}_A - \mathbf{R}_B|$ is the distance of the atoms A and B , s_n is a global scaling factor adjusted to the exchange-correlation functional, and f_{damp} is a damping function to avoid near-singularities at small distances and double-counting effects at intermediate distances. In DFT-D3 [27], the sum over n is truncated after $n = 8$, and the dispersion coefficients are calculated by time-dependent density functional theory.

2.2.3 Basis Set Expansion

The Kohn–Sham equations (2.17) are usually solved by representing the Kohn–Sham orbitals $\theta_i(\mathbf{r})$ as linear combinations of a finite set of n known basis functions $\phi_j(\mathbf{r})$:

$$\theta_i(\mathbf{r}) = \sum_{j=1}^n C_{ij} \phi_j(\mathbf{r}). \quad (2.23)$$

This allows to transform the Kohn–Sham equations from their integro-differential form into a matrix representation:

$$\mathbf{K}\mathbf{C} = \mathbf{S}\mathbf{C}\boldsymbol{\epsilon}. \quad (2.24)$$

In this equation, \mathbf{K} is the Kohn–Sham matrix with the elements

$$K_{ij} = \left\langle \phi_i(\mathbf{r}) \left| -\frac{\hbar^2}{2m_e} \nabla^2 + v_{\text{ext}}(\mathbf{r}) + \frac{1}{4\pi\epsilon_0} \int \frac{\rho(\mathbf{r}_1)}{|\mathbf{r} - \mathbf{r}_1|} d\mathbf{r}_1 + \frac{\delta E_{\text{xc}}[\rho(\mathbf{r})]}{\delta \rho(\mathbf{r})} \right| \phi_j(\mathbf{r}) \right\rangle, \quad (2.25)$$

\mathbf{S} is the overlap matrix with the elements

$$S_{ij} = \langle \phi_i(\mathbf{r}) | \phi_j(\mathbf{r}) \rangle, \quad (2.26)$$

\mathbf{C} is the matrix of the coefficients C_{ij} from the basis expansion (2.23), and $\boldsymbol{\epsilon}$ is a diagonal matrix with the orbital energies ϵ_i on the main diagonal. In doing so, the problem of finding the Kohn–Sham orbitals $\theta_i(\mathbf{r})$ is reduced to the task of determining the coefficients C_{ij} . Equation (2.24) possesses the form of a generalized eigenvalue problem, but since the Kohn–Sham matrix \mathbf{K} depends on the coefficients \mathbf{C} , an iterative procedure is needed: An initial guess for the coefficients \mathbf{C} is taken, the Kohn–Sham matrix \mathbf{K} is evaluated using these coefficients, new coefficients \mathbf{C} are calculated by solving the generalized eigenvalue problem, and this process is repeated

until the coefficients do not change anymore. This means that they are self-consistent, and the approach is, therefore, called self-consistent field (SCF) method.

Several choices for the basis functions $\phi_i(\mathbf{r})$ have been proposed. Very common in quantum chemistry are contracted Gaussian type orbitals (GTOs) of the general form

$$\phi(\mathbf{r}) = N\xi(\mathbf{r} - \mathbf{r}_0) \sum_{k=1}^m d_k \exp(-\zeta_k |\mathbf{r} - \mathbf{r}_0|^2), \quad (2.27)$$

which try to mimic the atomic orbitals of the individual atoms. Here, N is a normalization constant, $\xi(\mathbf{r} - \mathbf{r}_0)$ contains the angular momentum dependence, and \mathbf{r}_0 is the center of the basis function, which usually coincides with the position of the corresponding nucleus. The orbital exponents ζ_k and the expansion coefficients d_k are optimized once when the basis set is created, but they remain fixed in the SCF procedure to solve Eq. (2.24). Advantages of GTO basis sets are the good results with small set sizes and the straight description of all electrons in the system. However, the basis functions are not generally orthogonal, which can lead to linear dependencies that cause problems in the SCF procedure. Moreover, one has to take care of the basis set superposition error and Pulay forces [29] due to the position dependence of the basis functions.

Another approach, which is very common in solid state physics, is the use of plane wave basis sets. The periodicity of a crystalline solid imposes the same periodicity on the electron density, suggesting to use basis functions of the general form

$$\phi(\mathbf{r}) = \frac{1}{\sqrt{\Omega}} \exp(i\mathbf{G} \cdot \mathbf{r}), \quad (2.28)$$

where Ω is the volume of the periodic cell, and the wave vector \mathbf{G} has to satisfy the periodic boundary conditions. Usually, the basis set expansion (2.23) contains all wave vectors up to a certain cutoff. Since the plane waves are independent of the nuclear positions, Pulay forces and the basis set superposition error do not occur. Furthermore, all basis functions are orthogonal, making the overlap matrix trivial. Although a plane wave basis set implies periodic boundary conditions, molecular calculations in the gas phase are possible by applying such a large cell that the periodic images do not interact. The drawback of this approach is that a large number of basis functions is actually used to describe the empty part of the system.

A major issue of plane waves is the very high cutoff that is required to describe the rapid oscillations of the wave function due to the nodal structure of the valence orbitals near the nuclei. To overcome this problem, it is very common to apply pseudopotentials. A pseudopotential combines the Coulomb potential of the nuclei and the effective interaction potential of the core electrons with the valence electrons, and it replaces the sole Coulomb attraction of the nuclei in the external potential (2.12). This softens the potential the valence electrons move in, and lower cutoffs are sufficient for an adequate description. On the other hand, the core electrons are not

treated explicitly anymore, but this is only a minor restriction for most chemical applications.

2.2.4 The Gaussian and Plane Waves Method

The Gaussian and plane waves method [30, 31] is a particular implementation of DFT available in the CP2K software package [32], aiming for efficient calculations of large systems containing several thousand atoms. Within this approach, the Kohn–Sham orbitals are expanded in terms of GTO basis functions, but an auxiliary basis of plane waves is used for a second representation of the electron density. To convert between these representations, the electron density in the GTO basis is mapped onto a real-space grid with a spacing determined by the plane wave cutoff, and the plane wave coefficients are obtained by a discrete Fourier transform. The pseudopotentials of Goedecker, Teter, and Hutter (GTH) [33–35] are employed to reduce the necessary cutoff in the plane wave basis (see Sect. 2.2.3). These pseudopotentials are norm-conserving and separable, and their dual-space Gaussian form allows for an analytic calculation of the corresponding matrix elements in the GTO basis set. Also the kinetic energy contributions to the Kohn–Sham matrix are evaluated in the GTO basis, but the Coulomb interaction and the exchange–correlation potential are more efficiently calculated in the plane wave representation of the electron density. This leads to a construction scheme of the Kohn–Sham matrix that scales linearly with the system size.

Due to the application of GTH pseudopotentials, the electron density vanishes at the positions of the nuclei except for hydrogen atoms. Since many GGA exchange–correlation functionals contain terms with the electron density in the denominator, this gives rise to numerical problems in the evaluation of the exchange–correlation potential near the nuclei, making the total energy dependent on the atom positions relative to the real-space grid imposed by the plane wave basis. To reduce this effect, several smoothing procedures have been developed [31].

The SCF method described in Sect. 2.2.3 relies on the diagonalization of a matrix. An alternative approach is the direct minimization of the electronic energy (2.16), rewritten with the basis set expansion (2.23). In this formulation, the energy $E(\mathbf{C})$ is a function of the expansion coefficients, and the orthonormality constraint is given by $\mathbf{C}^T \mathbf{S} \mathbf{C} = \mathbf{I}$, where \mathbf{C} and \mathbf{S} are defined in Sect. 2.2.3, and \mathbf{I} is the identity matrix of the appropriate size. A minimization with this nonlinear constraint would require to follow a curved geodesic, but this can be avoided [36] by introducing a new set of variables \mathbf{X} that fulfill the linear constraint

$$\mathbf{X}^T \mathbf{S} \mathbf{C}_0 = \mathbf{0}, \quad (2.29)$$

where \mathbf{C}_0 are constant initial coefficients that satisfy the original constraint $\mathbf{C}_0^T \mathbf{S} \mathbf{C}_0 = \mathbf{I}$. The coefficients \mathbf{C} are related to the new variables \mathbf{X} by

$$\mathbf{C} = \mathbf{C}_0 \cos(\mathbf{U}) + \mathbf{X}\mathbf{U}^{-1} \sin(\mathbf{U}), \quad \text{with} \quad \mathbf{U} = (\mathbf{X}^T \mathbf{S} \mathbf{X})^{\frac{1}{2}}. \quad (2.30)$$

With a linear constraint, any standard minimization algorithm such as the conjugate gradient method or direct inversion in the iterative subspace (DIIS) [37] can be employed.

In the CP2K software package, this approach is available as orbital transformation (OT) method. If conjugate gradients are used with an extensive line search, convergence is guaranteed, leading to a procedure that can handle also cases which are problematic within the traditional diagonalization approach. Furthermore, the OT method is often faster than diagonalization [36].

2.3 Molecular Dynamics

Within the Born–Oppenheimer approximation, the nuclei obey the nuclear Schrödinger equation, which was given in its time-independent form in Eq. (2.9). The time-dependent form reads as

$$\left(- \sum_{A=1}^M \frac{\hbar^2}{2M_A} \nabla_A^2 + E_k(\mathbf{R}) \right) \chi_k(\mathbf{R}, t) = i\hbar \frac{\partial}{\partial t} \chi_k(\mathbf{R}, t). \quad (2.31)$$

For basic cases such as, e.g., the harmonic oscillator (see Sect. 2.4.1), it can be solved analytically. For larger systems, it can be simplified by approximating the nuclei as classical point particles. For this purpose, the complex nuclear wave function is rewritten as

$$\chi_k(\mathbf{R}, t) = B_k(\mathbf{R}, t) \exp \left(i \frac{S_k(\mathbf{R}, t)}{\hbar} \right) \quad (2.32)$$

with real functions $B_k(\mathbf{R}, t)$ (amplitude) and $S_k(\mathbf{R}, t)$ (phase). Applying this ansatz to Eq. (2.31) and separating the real and imaginary parts results in two coupled equations for amplitude and phase:

$$\frac{\partial}{\partial t} B_k(\mathbf{R}, t) + \sum_{A=1}^M \frac{1}{M_A} \left(\nabla_A B_k(\mathbf{R}, t) \nabla_A S_k(\mathbf{R}, t) + \frac{1}{2} B_k(\mathbf{R}, t) \nabla_A^2 S_k(\mathbf{R}, t) \right) = 0, \quad (2.33)$$

$$\frac{\partial}{\partial t} S_k(\mathbf{R}, t) + \sum_{A=1}^M \frac{1}{2M_A} (\nabla_A S_k(\mathbf{R}, t))^2 + E_k(\mathbf{R}) = \hbar^2 \sum_{A=1}^M \frac{1}{2M_A} \frac{\nabla_A^2 B_k(\mathbf{R}, t)}{B_k(\mathbf{R}, t)}. \quad (2.34)$$

Equation (2.33) can be interpreted as a continuity equation that ensures the conservation of the probability density $|\chi_k(\mathbf{R}, t)|^2$. In Eq. (2.34), the right-hand side vanishes in the classical limit $\hbar \rightarrow 0$, and the Hamilton–Jacobi equation of classical

mechanics remains:

$$\frac{\partial}{\partial t} S_k(\mathbf{R}, t) + \sum_{A=1}^M \frac{1}{2M_A} (\nabla_A S_k(\mathbf{R}, t))^2 + E_k(\mathbf{R}) = \frac{\partial}{\partial t} S_k(\mathbf{R}, t) + H_k(\mathbf{R}, \mathbf{P}) = 0 \quad (2.35)$$

with the momenta $\mathbf{P} = \{\mathbf{P}_A\}$, $\mathbf{P}_A(t) = \nabla_A S_k(\mathbf{R}, t)$, and the Hamilton function $H_k(\mathbf{R}, \mathbf{P}) = T(\mathbf{P}) + E_k(\mathbf{R})$, where $T(\mathbf{P})$ is the kinetic energy. This can be transformed to the Newtonian equations of motion

$$\frac{d}{dt} \mathbf{P}_A(t) = M_A \frac{d^2}{dt^2} \mathbf{R}_A(t) = -\nabla_A E_k(\mathbf{R}(t)). \quad (2.36)$$

This means that the nuclei move according to classical mechanics in the potential that is provided by the electronic energy $E_k(\mathbf{R})$, suggesting the following procedure to study the time evolution of a molecular system: the nuclei are propagated according to Eq. (2.36), and at any particular time t , the electronic energy and its gradient are obtained by solving the time-independent electronic Schrödinger equation (2.6) for the current nuclear configuration $\mathbf{R}(t)$. This approach is called Born–Oppenheimer molecular dynamics (BOMD). The AIMD simulations performed in the course of this thesis are BOMD simulations.

The Newtonian equations of motion (2.36) are usually solved by numerical methods that introduce a discrete timestep Δt . In the Verlet algorithm [38], the nuclear coordinates are expanded in Taylor series up to third order:

$$\mathbf{R}_A(t + \Delta t) = \mathbf{R}_A(t) + \Delta t \frac{d}{dt} \mathbf{R}_A(t) + \frac{1}{2} \Delta t^2 \frac{d^2}{dt^2} \mathbf{R}_A(t) + \frac{1}{6} \Delta t^3 \frac{d^3}{dt^3} \mathbf{R}_A(t) + \mathcal{O}(\Delta t^4), \quad (2.37)$$

$$\mathbf{R}_A(t - \Delta t) = \mathbf{R}_A(t) - \Delta t \frac{d}{dt} \mathbf{R}_A(t) + \frac{1}{2} \Delta t^2 \frac{d^2}{dt^2} \mathbf{R}_A(t) - \frac{1}{6} \Delta t^3 \frac{d^3}{dt^3} \mathbf{R}_A(t) + \mathcal{O}(\Delta t^4). \quad (2.38)$$

Adding these two equations and rearranging the terms leads to

$$\mathbf{R}_A(t + \Delta t) = 2\mathbf{R}_A(t) - \mathbf{R}_A(t - \Delta t) + \frac{1}{M_A} \Delta t^2 \mathbf{F}_A(t) + \mathcal{O}(\Delta t^4), \quad (2.39)$$

where the forces $\mathbf{F}_A(t) = M_A \ddot{\mathbf{R}}_A(t) = -\nabla_A E_k(\mathbf{R}(t))$ are introduced. The nuclear velocities $\mathbf{V}_A(t) = \dot{\mathbf{R}}_A(t)$ are eliminated in this derivation, but it is often desirable to know them, e.g., to calculate the kinetic energy. Therefore, it is more convenient to apply the velocity form of the Verlet algorithm [39], where coordinates and velocities are given by

$$\mathbf{R}_A(t + \Delta t) = \mathbf{R}_A(t) + \Delta t \mathbf{V}_A(t) + \frac{1}{2M_A} \Delta t^2 \mathbf{F}_A(t), \quad (2.40)$$

$$\mathbf{V}_A(t + \Delta t) = \mathbf{V}_A(t) + \frac{1}{2M_A} \Delta t (\mathbf{F}_A(t) + \mathbf{F}_A(t + \Delta t)). \quad (2.41)$$

It can be shown that this formulation is equivalent to the original Verlet method, but it directly delivers the velocities in each step of the simulation. The complete BOMD procedure starting from certain initial coordinates $\mathbf{R}(0)$ and velocities $\mathbf{V}(0)$ now reads as follows: The coordinates $\mathbf{R}(t)$ are used to calculate the forces $\mathbf{F}(t)$ by solving the time-independent electronic Schrödinger equation for these coordinates (e.g., by applying DFT, see Sect. 2.2), the new coordinates $\mathbf{R}(t + \Delta t)$ are calculated by Eq. (2.40), they are used to obtain the new forces $\mathbf{F}(t + \Delta t)$ by solving again the electronic Schrödinger equation, and the new velocities $\mathbf{V}(t + \Delta t)$ are finally given by Eq. (2.41). This procedure has to be repeated until a reasonable part of the nuclear phase space is sampled.

Since BOMD on the basis of the Newtonian equations of motion (2.36) conserves the total energy, a trajectory in the microcanonical or *NVE* ensemble is generated. For comparison with experiments, where usually the temperature is controlled, it is, however, desirable to run simulations in the canonical or *NVT* ensemble. For this purpose, a thermostat has to be applied. A very common choice is the Nosé–Hoover thermostat [40–42], which adds a heat bath by introducing an additional degree of freedom to the system. This “heat bath particle” follows a specific potential so that the original degrees of freedom sample the *NVT* ensemble. To handle also difficult cases, the concept has been extended to the Nosé–Hoover thermostat chain [43], where the heat bath is coupled to another heat bath. Introducing further heat baths that are successively connected to each other finally leads to a linear chain of *K* thermostats with the following equations of motion:

$$M_A \ddot{\mathbf{R}}_A(t) = -\nabla_A E_k(\mathbf{R}(t)) - M_A \dot{\xi}_1(t) \dot{\mathbf{R}}_A(t), \quad (2.42)$$

$$Q_1 \ddot{\xi}_1(t) = \sum_{A=1}^M M_A \dot{\mathbf{R}}_A(t)^2 - g k_B T - Q_1 \dot{\xi}_1(t) \dot{\xi}_2(t), \quad (2.43)$$

$$Q_i \ddot{\xi}_i(t) = Q_{i-1} \dot{\xi}_{i-1}(t)^2 - k_B T - Q_i \dot{\xi}_i(t) \dot{\xi}_{i+1}(t), \quad i = 2, \dots, K-1, \quad (2.44)$$

$$Q_K \ddot{\xi}_K(t) = Q_{K-1} \dot{\xi}_{K-1}(t)^2 - k_B T. \quad (2.45)$$

Here, *T* is the desired average temperature, and *g* is the number of degrees of freedom to which the thermostat chain is coupled (*g* = 3*M* if no constraints are imposed on the nuclear coordinates). Each thermostat has a coordinate $\xi_i(t)$ and a mass-like parameter Q_i , which is chosen as

$$Q_1 = g k_B T \tau^2, \quad Q_i = k_B T \tau^2, \quad i = 2, \dots, K. \quad (2.46)$$

The coupling time constant τ should be in the order of the timescale of the nuclear motions. Since the forces in the equations of motion explicitly depend on the

velocities, the velocity Verlet algorithm cannot be applied directly. It is possible to solve Eq. (2.41) iteratively, but also explicit reversible integrators have been developed [44] on the basis of the Liouville operator, multiple timestep schemes, and higher order Yoshida–Suzuki integration [45, 46]. For the NVE ensemble, these reduce to the velocity Verlet method.

For the equilibration of an MD simulation, it is convenient to use an individual Nosé–Hoover thermostat chain for each degree of freedom (massive thermostat). This significantly reduces the equilibration time and helps to excite even stiff vibrational modes that are only loosely coupled to all other modes of the system, as it is required to fulfill the equipartition theorem.

2.4 Vibrational Spectroscopy

2.4.1 The Harmonic Oscillator

As discussed in Sect. 2.1, the Born–Oppenheimer approximation decouples the electronic from the nuclear motion in a molecular system. The nuclei move on the $3M$ -dimensional potential energy surface that is determined by the electronic structure. In a typical stable molecule, this potential has distinct minima and the molecule performs oscillations around these minima.

For simplicity, a one-dimensional potential $V(x)$ with a minimum at $x = 0$ is considered in the following. The Taylor series around $x = 0$ reads as

$$V(x) = V(0) + V'(0)x + \frac{1}{2}V''(0)x^2 + \frac{1}{6}V'''(0)x^3 + \dots \quad (2.47)$$

The first term is a constant offset and the potential can always be transformed to make this offset vanish by choosing an appropriate energy zero point. Since the potential has a minimum at $x = 0$, also the second term is zero. The first non-vanishing term is the harmonic potential

$$V(x) = \frac{1}{2}kx^2, \quad (2.48)$$

where the second derivative of the potential is identified with the force constant k . This means that the first approximation to an arbitrarily shaped potential is given by (2.48) in the vicinity of a minimum. In particular, also the nuclear motion in a molecule can approximately be described within a multidimensional harmonic potential.

In classical mechanics (cf. Eq. (2.36)), a particle of mass m moving in the harmonic potential (2.48) fulfills the differential equation

$$m\ddot{x}(t) + kx(t) = 0. \quad (2.49)$$

It can be shown that the general solution of this differential equation is

$$x(t) = x_0 \cos\left(\sqrt{\frac{k}{m}}t + \varphi\right) = x_0 \cos(\omega_0 t + \varphi), \quad (2.50)$$

where the eigenfrequency $\omega_0 = \sqrt{k/m}$ is introduced. This means that the particle performs a harmonic vibration with the constant angular frequency ω_0 . The amplitude x_0 and the phase φ are determined by the initial conditions.

In quantum mechanics (cf. Eq. (2.9)), the corresponding differential equation reads as

$$\left(-\frac{\hbar^2}{2m} \frac{d^2}{dx^2} + \frac{1}{2} kx^2\right) \chi_n(x) = \varepsilon_n \chi_n(x). \quad (2.51)$$

If $\omega_0 = \sqrt{k/m}$ is set as in the classical case, the eigenfunctions of the quantum harmonic oscillator are given by

$$\chi_n(x) = \frac{1}{\sqrt{2^n n!}} \sqrt{\frac{m\omega_0}{\pi \hbar}} H_n\left(\sqrt{\frac{m\omega_0}{\hbar}} x\right) \exp\left(-\frac{1}{2} \frac{m\omega_0}{\hbar} x^2\right) \quad (2.52)$$

with the Hermite polynomials

$$H_n(x) = (-1)^n \exp(x^2) \frac{d^n}{dx^n} \exp(-x^2). \quad (2.53)$$

The energy eigenvalues are

$$\varepsilon_n = \hbar\omega_0 \left(n + \frac{1}{2}\right), \quad n \geq 0. \quad (2.54)$$

The quantum harmonic oscillator can only take discrete energy values with a constant spacing of $\hbar\omega_0$. Even the ground state has the non-vanishing energy $\varepsilon_0 = \hbar\omega_0/2$, which is called zero-point energy.

Both types of harmonic oscillators are easily extended to the multidimensional case, since the multidimensional harmonic potential

$$V(\mathbf{x}) = \frac{1}{2} \mathbf{x}^T \mathbf{k} \mathbf{x} \quad (2.55)$$

can always be written as a sum of one-dimensional harmonic potentials if the force matrix \mathbf{k} is diagonal. If the force matrix \mathbf{k} is not diagonal, an appropriate transformation to the system of normal coordinates has to be applied beforehand. In such a separable potential, the classical harmonic oscillator performs a harmonic vibration (2.50) along each normal coordinate. The total wave function of the quantum harmonic oscillator is the product of the one-dimensional wave functions (2.52), and its energy is the sum of the one-dimensional energy eigenvalues (2.54).

2.4.2 Infrared Absorption

The nuclei in a molecule generally follow the laws of quantum mechanics, so they can only take discrete eigenstates with certain energy values, as discussed for the harmonic approximation to the potential energy surface in Sect. 2.4.1. A change from one eigenstate to another one is possible by the absorption or emission of electromagnetic radiation, the energy of which is equal to the energy difference between the two states. For the nuclear vibrations in a molecule, these energy differences are typically in the range of 10^{-21} to 10^{-19} J, corresponding to the IR region of the electromagnetic spectrum. This leads to the experimental technique of IR spectroscopy: a chemical substance is irradiated with IR radiation and its absorption is measured in dependence of its energy. The resulting spectrum shows peaks at positions characteristic for the molecular structure. For a harmonic oscillator, e.g., the peak is located at the difference $\hbar\sqrt{k/m}$ between two subsequent states, so its position is directly related to the force constant.

Beside the peak positions, also the intensities are an important property of IR spectra. Their theoretical values can be derived [47] by applying Fermi's golden rule [48, 49]

$$W_{i \rightarrow f} = \frac{1}{\hbar^2} |\langle v_f | \mathcal{H}' | v_i \rangle|^2 \rho_N(v_f), \quad (2.56)$$

which gives the transition rate $W_{i \rightarrow f}$ for the transition from state $|v_i\rangle$ to state $|v_f\rangle$ when the perturbation \mathcal{H}' by electromagnetic radiation with a density of photon states per frequency range $\rho_N(\nu)$ is applied to the system. Within the dipole approximation, the perturbation is

$$\langle v_f | \mathcal{H}' | v_i \rangle = -\langle v_f | \bar{\boldsymbol{\mu}}(\mathbf{Q}) \cdot \mathbf{E} | v_i \rangle = -\langle v_f | \bar{\boldsymbol{\mu}}(\mathbf{Q}) | v_i \rangle \cdot \mathbf{E}_0 \quad (2.57)$$

where $\bar{\boldsymbol{\mu}}(\mathbf{Q})$ is the molecular dipole moment depending on the mass-weighted normal coordinates \mathbf{Q} (the overbar indicates the expectation value over the electronic coordinates), and \mathbf{E} is the electric field vector of the radiation, which is assumed to be constant over the extent of the molecule with an average amplitude \mathbf{E}_0 . For the evaluation of the transition dipole matrix elements, the translational and rotational degrees of freedom are separated and the classical average over all rotational states is taken. Within the harmonic approximation, the harmonic oscillator wave functions (2.52) are used for the remaining $g = 3M - 6$ ($g = 3M - 5$ in a linear molecule) vibrational degrees of freedom. The molecular dipole moment is expanded in a Taylor series around the minimum of the potential energy surface up to first order:

$$\bar{\boldsymbol{\mu}}(\mathbf{Q}) = \bar{\boldsymbol{\mu}}_0 + \sum_{k=1}^g \left(\frac{\partial \bar{\boldsymbol{\mu}}(\mathbf{Q})}{\partial Q_k} \right)_0 Q_k. \quad (2.58)$$

With all these assumptions, analytic expressions for the transition dipole matrix elements can be found, and the integral absorption coefficient for the transition from

the ground state to the first excited state in the harmonic oscillator corresponding to mode k is given by [47]

$$A_k = \frac{1}{4\pi\epsilon_0} \frac{N_A}{3c^2} \pi \left(\frac{\partial \bar{\mu}(\mathbf{Q})}{\partial Q_k} \right)_0^2. \quad (2.59)$$

This shows that a particular vibrational mode appears as a peak in the IR spectrum of a molecule if the dipole moment changes along this mode.

Equation (2.59) can be used to estimate IR spectra by static quantum chemical calculations within the harmonic approximation to the potential energy surface: a geometry optimization is performed to find the minimum of the potential energy surface, the Hessian matrix of the potential energy at this point is the force matrix in (2.55), the force matrix is diagonalized to get the normal coordinates and the vibrational frequencies, and the dipole moment derivatives along the normal coordinates are calculated to obtain IR intensities according to (2.59).

For chiral molecules, the absorption is not the same if left and right circularly polarized IR radiation are compared. The difference between these two cases is measured in VCD spectroscopy. For a theoretical model of VCD intensities, the interaction of the molecular magnetic moment \mathbf{m} with the magnetic field of the electromagnetic radiation has to be taken into account. In this way, it is found that the VCD intensity for the transition from state $|i\rangle$ to state $|f\rangle$ is proportional to the rotational strength [50]

$$R_{i \rightarrow f} = \text{Im} \left(\langle i | \hat{\mu} | f \rangle \langle f | \hat{\mathbf{m}} | i \rangle \right), \quad (2.60)$$

where $\hat{\mu}$ and $\hat{\mathbf{m}}$ are the electric dipole and magnetic dipole operators, respectively. The magnetic transition moment needs special care, since the matrix elements $\langle f | \hat{\mathbf{m}} | i \rangle$ always vanish within the Born–Oppenheimer approximation. This can be circumvented by magnetic field perturbation theory [51–54] or nuclear velocity perturbation theory [55–61], allowing to calculate VCD spectra by static calculations within the harmonic approximation.

2.4.3 Raman Scattering

Beside absorption and emission, the scattering of electromagnetic radiation is another physical process that can change the quantum state of a molecule. When photons interact with molecules, most of them are scattered elastically, so the scattered photons have the same energy as the incident photons and the molecular quantum state remains unchanged (Rayleigh scattering). However, a small fraction of the photons is scattered inelastically, meaning that the molecule switches to another quantum state and the photon energy changes by the energy difference of the two molecular states. This effect is named Raman scattering after Chandrasekhara Raman, who first verified it experimentally [62], five years after the theoretical prediction by Adolf

Smekal [63]. If the molecule switches to a state higher in energy and the photon energy is reduced, the process is called Stokes Raman scattering. If the molecule switches to a state lower in energy and the photon energy is increased, the process is called anti-Stokes Raman scattering.

The effect of Raman scattering is used in Raman spectroscopy as an alternative to IR spectroscopy for the investigation of molecular vibrations. Due to the low efficiency of the Raman scattering process and the dependence of the scattering cross section on the fourth power of the photon energy, it is common to use high intensity lasers in the visible region of the electromagnetic spectrum for the irradiation of the sample. The intensity of the scattered radiation is measured in dependence of its energy, and the peak positions are recorded relative to the incident radiation, so they relate to energy differences between vibrational states, and Raman spectra can directly be compared to IR spectra.

Theoretical values for Raman intensities can be obtained from Placzek's classical theory of polarizability [64]. The electric field of the incident radiation induces a dipole moment in the molecule, and within classical electrodynamics, the scattered intensity is proportional to the square of the induced dipole moment. The expectation value of the induced dipole moment μ_{fi}^{ind} is determined quantum mechanically by evaluation of the corresponding polarizability matrix elements,

$$\langle \mu_{fi}^{\text{ind}} \rangle = \langle v_f | \tilde{\alpha}(\mathbf{Q}) | v_i \rangle \mathbf{E}_0, \quad (2.61)$$

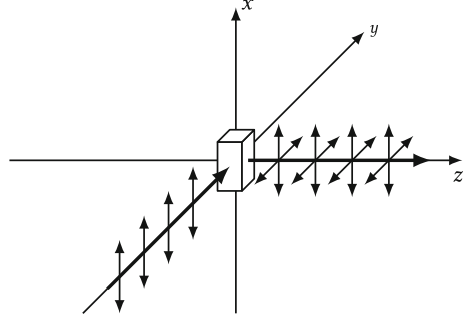
where it is assumed again that the electric field is constant over the extent of the molecule with an average amplitude \mathbf{E}_0 . The polarizability tensor $\tilde{\alpha}(\mathbf{Q})$ (the overbar indicates the expectation value over the electronic coordinates) is expanded in a Taylor series analogous to (2.58):

$$\tilde{\alpha}(\mathbf{Q}) = \tilde{\alpha}_0 + \sum_{k=1}^g \left(\frac{\partial \tilde{\alpha}(\mathbf{Q})}{\partial Q_k} \right)_0 Q_k. \quad (2.62)$$

This allows to derive analytic expressions for the Raman intensities of individual vibrational modes [47]. An important parameter is, however, the scattering geometry employed in the measurement setup. A common choice for theoretical investigations is shown in Fig. 2.1: the incident light beam propagates along the y axis and is polarized along the x axis. The detector for the scattered light is located on the z axis and is equipped with a polarization filter to measure the x polarized intensity I^{\parallel} and the y polarized intensity I^{\perp} . If the molecule is fixed with respect to the laboratory coordinate system, the differential Raman scattering cross sections for the Stokes line of vibrational mode k in this setup are given by

$$I_k^{\parallel} = \frac{\pi^2}{\varepsilon_0^2} (\tilde{\nu}_{\text{in}} - \tilde{\nu}_k)^4 \frac{h}{8 \pi^2 c \tilde{\nu}_k} \left(\frac{\partial \tilde{\alpha}_{xx}(\mathbf{Q})}{\partial Q_k} \right)_0^2 \frac{1}{1 - \exp\left(-\frac{hc\tilde{\nu}_k}{k_B T}\right)} \quad (2.63)$$

Fig. 2.1 Measurement setup for Raman spectra. The incident light beam propagates along the y axis and is polarized along the x axis. The light scattered along the z axis is detected with a polarization filter for either x polarized or y polarized light



and

$$I_k^\perp = \frac{\pi^2}{\varepsilon_0^2} (\tilde{\nu}_{\text{in}} - \tilde{\nu}_k)^4 \frac{h}{8 \pi^2 c \tilde{\nu}_k} \left(\frac{\partial \tilde{\alpha}_{xy}(\mathbf{Q})}{\partial Q_k} \right)_0^2 \frac{1}{1 - \exp\left(-\frac{hc\tilde{\nu}_k}{k_B T}\right)}, \quad (2.64)$$

where $\tilde{\nu}_{\text{in}}$ is the wavenumber of the incident radiation, $\tilde{\nu}_k$ is the wavenumber corresponding to vibrational mode k , and T is the temperature. This shows that a particular vibrational mode appears as a peak in the Raman spectrum of a molecule if the polarizability changes along this mode. If the molecule is randomly orientated with respect to the laboratory frame, the classical averages of the polarizability tensor components have to be taken. This results in

$$I_k^\parallel = \frac{\pi^2}{\varepsilon_0^2} (\tilde{\nu}_{\text{in}} - \tilde{\nu}_k)^4 \frac{h}{8 \pi^2 c \tilde{\nu}_k} \frac{45a_k^2 + 4\gamma_k^2}{45} \frac{1}{1 - \exp\left(-\frac{hc\tilde{\nu}_k}{k_B T}\right)} \quad (2.65)$$

and

$$I_k^\perp = \frac{\pi^2}{\varepsilon_0^2} (\tilde{\nu}_{\text{in}} - \tilde{\nu}_k)^4 \frac{h}{8 \pi^2 c \tilde{\nu}_k} \frac{3\gamma_k^2}{45} \frac{1}{1 - \exp\left(-\frac{hc\tilde{\nu}_k}{k_B T}\right)} \quad (2.66)$$

with the isotropic polarizability derivative

$$a_k = \frac{1}{3} \left(\left(\frac{\partial \tilde{\alpha}_{xx}(\mathbf{Q})}{\partial Q_k} \right)_0 + \left(\frac{\partial \tilde{\alpha}_{yy}(\mathbf{Q})}{\partial Q_k} \right)_0 + \left(\frac{\partial \tilde{\alpha}_{zz}(\mathbf{Q})}{\partial Q_k} \right)_0 \right) \quad (2.67)$$

and the anisotropy

$$\begin{aligned} \gamma_k^2 = & \frac{1}{2} \left(\left(\frac{\partial \tilde{\alpha}_{xx}(\mathbf{Q})}{\partial Q_k} \right)_0 - \left(\frac{\partial \tilde{\alpha}_{yy}(\mathbf{Q})}{\partial Q_k} \right)_0 \right)^2 + \frac{1}{2} \left(\left(\frac{\partial \tilde{\alpha}_{yy}(\mathbf{Q})}{\partial Q_k} \right)_0 - \left(\frac{\partial \tilde{\alpha}_{zz}(\mathbf{Q})}{\partial Q_k} \right)_0 \right)^2 \\ & + \frac{1}{2} \left(\left(\frac{\partial \tilde{\alpha}_{zz}(\mathbf{Q})}{\partial Q_k} \right)_0 - \left(\frac{\partial \tilde{\alpha}_{xx}(\mathbf{Q})}{\partial Q_k} \right)_0 \right)^2 + 3 \left(\frac{\partial \tilde{\alpha}_{xy}(\mathbf{Q})}{\partial Q_k} \right)_0^2 + 3 \left(\frac{\partial \tilde{\alpha}_{yz}(\mathbf{Q})}{\partial Q_k} \right)_0^2 + 3 \left(\frac{\partial \tilde{\alpha}_{zx}(\mathbf{Q})}{\partial Q_k} \right)_0^2. \end{aligned} \quad (2.68)$$

An important quantity related to the scattering intensities is the depolarization ratio

$$\rho_k = \frac{I_k^\perp}{I_k^\parallel}. \quad (2.69)$$

For vibrations that transform as the totally symmetric irreducible representation of the molecular point group, it can be lower than 0.75, but it is 0.75 in all other cases.

Analogous to IR spectra, these expressions can be used to estimate Raman spectra by static quantum chemical calculations within the harmonic approximation. They just require the calculation of the polarizability derivatives along the normal coordinates.

References

1. E. Schrödinger, Phys. Rev. **28**, 1049–1070 (1926)
2. I. Levine, *Quantum Chemistry* (Pearson Prentice Hall, Upper Saddle River, 2009)
3. A. Szabo, N. Ostlund, *Modern Quantum Chemistry: Introduction to Advanced Electronic Structure Theory*, Dover Books on Chemistry Series (Dover Publications, Mineola, 1996)
4. F. Jensen, *Introduction to Computational Chemistry* (Wiley, Chichester, 2006)
5. D. Marx, J. Hutter, *Ab Initio Molecular Dynamics: Basic Theory and Advanced Methods* (Cambridge University Press, Cambridge, 2009)
6. M. Born, R. Oppenheimer, Ann. Phys. **389**, 457–484 (1927)
7. P. Hohenberg, W. Kohn, Phys. Rev. **136**, B864–B871 (1964)
8. W. Kohn, L.J. Sham, Phys. Rev. **140**, A1133–A1138 (1965)
9. F. Bloch, Z. Phys. **57**, 545–555 (1929)
10. P.A.M. Dirac, Math. Proc. Camb. **26**, 376–385 (1930)
11. S.H. Vosko, L. Wilk, M. Nusair, Can. J. Phys. **58**, 1200–1211 (1980)
12. J.C. Slater, Phys. Rev. **81**, 385–390 (1951)
13. A.D. Becke, Phys. Rev. A **38**, 3098–3100 (1988)
14. C. Lee, W. Yang, R.G. Parr, Phys. Rev. B **37**, 785–789 (1988)
15. J.P. Perdew, J.A. Chevary, S.H. Vosko, K.A. Jackson, M.R. Pederson, D.J. Singh, C. Fiolhais, Phys. Rev. B **46**, 6671–6687 (1992)
16. J.P. Perdew, K. Burke, M. Ernzerhof, Phys. Rev. Lett. **77**, 3865–3868 (1996)
17. J. Tao, J.P. Perdew, V.N. Staroverov, G.E. Scuseria, Phys. Rev. Lett. **91**, 146401 (2003)
18. A.D. Becke, J. Chem. Phys. **98**, 5648–5652 (1993)
19. P.J. Stephens, F.J. Devlin, C.F. Chabalowski, M.J. Frisch, J. Phys. Chem. **98**, 11623–11627 (1994)
20. C. Adamo, V. Barone, J. Chem. Phys. **110**, 6158–6170 (1999)
21. V.N. Staroverov, G.E. Scuseria, J. Tao, J.P. Perdew, J. Chem. Phys. **119**, 12129–12137 (2003)
22. D.C. Langreth, M. Dion, H. Rydberg, E. Schröder, P. Hyldgaard, B.I. Lundqvist, Int. J. Quantum Chem. **101**, 599–610 (2005)
23. T. Sato, T. Tsuneda, K. Hirao, Mol. Phys. **103**, 1151–1164 (2005)
24. O.A. von Lilienfeld, I. Tavernelli, U. Rothlisberger, D. Sebastiani, Phys. Rev. Lett. **93**, 153004 (2004)
25. Y.Y. Sun, Y.-H. Kim, K. Lee, S.B. Zhang, J. Chem. Phys. **129**, 154102 (2008)
26. S. Grimme, J. Comput. Chem. **27**, 1787–1799 (2006)
27. S. Grimme, J. Antony, S. Ehrlich, H. Krieg, J. Chem. Phys. **132**, 154104 (2010)
28. S. Grimme, S. Ehrlich, L. Goerigk, J. Comput. Chem. **32**, 1456–1465 (2011)
29. P. Pulay, Mol. Phys. **17**, 197–204 (1969)

30. G. Lippert, M. Parrinello, J. Hutter, *Mol. Phys.* **92**, 477–488 (1997)
31. J. VandeVondele, M. Krack, F. Mohamed, M. Parrinello, T. Chassaing, J. Hutter, *Comput. Phys. Commun.* **167**, 103–128 (2005)
32. J. Hutter, M. Iannuzzi, F. Schiffmann, J. VandeVondele, *WIREs Comput. Mol. Sci.* **4**, 15–25 (2014)
33. S. Goedecker, M. Teter, J. Hutter, *Phys. Rev. B* **54**, 1703–1710 (1996)
34. C. Hartwigsen, S. Goedecker, J. Hutter, *Phys. Rev. B* **58**, 3641–3662 (1998)
35. M. Krack, *Theor. Chem. Acc.* **114**, 145–152 (2005)
36. J. VandeVondele, J. Hutter, *J. Chem. Phys.* **118**, 4365–4369 (2003)
37. P. Pulay, *J. Comput. Chem.* **3**, 556–560 (1982)
38. L. Verlet, *Phys. Rev.* **159**, 98–103 (1967)
39. W.C. Swope, H.C. Andersen, P.H. Berens, K.R. Wilson, *J. Chem. Phys.* **76**, 637–649 (1982)
40. S. Nosé, *J. Chem. Phys.* **81**, 511–519 (1984)
41. S. Nosé, *Mol. Phys.* **52**, 255–268 (1984)
42. W.G. Hoover, *Phys. Rev. A* **31**, 1695–1697 (1985)
43. G.J. Martyna, M.L. Klein, M. Tuckerman, *J. Chem. Phys.* **97**, 2635–2643 (1992)
44. G.J. Martyna, M.E. Tuckerman, D.J. Tobias, M.L. Klein, *Mol. Phys.* **87**, 1117–1157 (1996)
45. H. Yoshida, *Phys. Lett. A* **150**, 262–268 (1990)
46. M. Suzuki, *J. Math. Phys.* **32**, 400–407 (1991)
47. J. Neugebauer, M. Reiher, C. Kind, B.A. Hess, *J. Comput. Chem.* **23**, 895–910 (2002)
48. P.A.M. Dirac, *Proc. R. Soc. Lond. Ser. A* **114**, 243–265 (1927)
49. J. Orear, E. Fermi, *Nuclear Physics: A Course Given by Enrico Fermi at the University of Chicago*, of Midway reprint, University of Chicago Press (1950)
50. C. Herrmann, M. Reiher, in *Atomistic Approaches in Modern Biology*, ed. by M. Reiher. Topics in Current Chemistry, vol. 268 (Springer, Heidelberg, 2007), pp. 85–132
51. P.J. Stephens, *J. Phys. Chem.* **89**, 748–752 (1985)
52. P.J. Stephens, *J. Phys. Chem.* **91**, 1712–1715 (1987)
53. J. Cheeseman, M. Frisch, F. Devlin, P. Stephens, *Chem. Phys. Lett.* **252**, 211–220 (1996)
54. V.P. Nicu, J. Neugebauer, S.K. Wolff, E.J. Baerends, *Theor. Chem. Acc.* **119**, 245–263 (2008)
55. L.A. Nafie, T.B. Freedman, *J. Chem. Phys.* **78**, 7108–7116 (1983)
56. L.A. Nafie, *J. Chem. Phys.* **79**, 4950–4957 (1983)
57. A. Buckingham, P. Fowler, P. Galwas, *Chem. Phys.* **112**, 1–14 (1987)
58. L.A. Nafie, *J. Chem. Phys.* **96**, 5687–5702 (1992)
59. L.A. Nafie, *J. Phys. Chem. A* **108**, 7222–7231 (2004)
60. A. Scherrer, R. Vuilleumier, D. Sebastiani, *J. Chem. Theory Comput.* **9**, 5305–5312 (2013)
61. A. Scherrer, F. Agostini, D. Sebastiani, E.K.U. Gross, R. Vuilleumier, *J. Chem. Phys.* **143**, 074106 (2015)
62. C. Raman, *Indian J. Phys.* **2**, 387–398 (1928)
63. A. Smekal, *Naturwissenschaften* **11**, 873–875 (1923)
64. G. Placzek, *Z. Phys.* **70**, 84–103 (1931)

Theoretical Modeling of Vibrational Spectra in the Liquid
Phase

Thomas, M.

2017, XXXIV, 184 p. 65 illus., 28 illus. in color.,

Hardcover

ISBN: 978-3-319-49627-6